Electronic and excitonic processes in light-emitting devices based on organic materials and colloidal quantum dots

P. O. Anikeeva, C. F. Madigan,* J. E. Halpert, M. G. Bawendi, and V. Bulović
Laboratory of Organic Optics and Electronics and Department of Chemistry, Massachusetts Institute of Technology, 77 Massachusetts Avenue, Cambridge, Massachusetts 02139, USA

(Received 26 March 2008; revised manuscript received 10 June 2008; published 27 August 2008)

We investigate the mechanism of operation of hybrid organic/colloidal quantum dot light emitting devices (QD-LEDs). Novel quantum dot (QD) deposition methods allow us to change the location of an emissive QD monolayer within a QD-LED multilayer structure. We find that the quantum efficiency of devices improves by >50% upon imbedding QD monolayers into the hole transporting layer <10 nm away from the interface between hole and electron transporting layers. We consider two possible mechanisms responsible for this improvement: one based on a charge injection model of the device operation and the other based on an exciton energy-transfer model. In order to differentiate between the two suggested mechanisms, we fabricate a set of structures that enable control over charge injection into colloidal QDs. We find that the dominant process limiting QD-LED efficiency is charging of the QDs by trapped electrons. We demonstrate that with the set of organic materials implemented in this study, device efficiency is increased by maximizing energy transfer from organics to QDs and by limiting direct charge injection that contributes to QD charging.

DOI: 10.1103/PhysRevB.78.085434 PACS number(s): 81.07.Pr, 85.35.Be, 73.63.Kv, 72.80.Le

I. INTRODUCTION

Hybrid light emitting devices[1] (LEDs) consisting of organic charge transporting layers and a colloidal quantum dot[2,3] (QD) emissive layer exhibit narrow electroluminescence (EL) spectra characteristic of colloidal QD luminescence. The manifested saturated color emission is particularly desirable in flat panel display applications and is broadly applicable to other technologies requiring high spectral quality lighting. Solubility of colloidal QDs in organic solvents facilitates the development of simple and scalable QD deposition methods such as microcontact printing that was shown to produce QD films with precise control of film thickness, pattern, and morphology.[4] Microcontact printing allows for fabrication of multiple QD-LEDs of different color on the same substrate by simply changing the QDs in the emissive layer.[5,6] Different color QDs can also be mixed in the LED emissive layer to produce QD-LEDs with precisely tuned colors.[6] To date, QD-LED emission across the visible and near-IR spectrum[5,7] has been demonstrated, however, we still find that the external quantum efficiency (EQE), i.e., the number of emitted photons per injected electron, differs for QD-LEDs of different color. The best published green, red, and orange QD-LEDs exhibit peak efficiencies in the range of 1%–2%,[8,9] while the efficiency of blue QD-LEDs is on the order of 0.4% for QDs of similar starting QD solution photoluminescence (PL) efficiencies.[6] In order to understand the differences in device performance and to systematically design more efficient QD-LEDs, in this paper we investigate the fundamental processes that govern the operation of QD-LEDs by observing performance variation in a variety of QD-LED structures. This systematic analysis leads to improved performance and optimized QD-LED structures.

An archetypical QD-LED consists of a transparent anode, on top of which an organic hole transporting layer is deposited, which is followed by a colloidal QD monolayer, an organic electron transporting layer, and a metallic cathode.[1,8] As of today two mechanisms have been proposed to explain electroluminescence of QD-LEDs.[5,6,10] By the first mechanism, carriers transported through organic charge transport layers are directly injected into QDs, where they can form excitons that can radiatively recombine. The second mechanism relies on the ability to form excitons on the organic molecules surrounding the QD film that then resonantly transfer the exciton energy to QDs. In the current study we assess the relative contribution of the two mechanisms to QD-LED electroluminescence (EL).

II. EXPERIMENT AND MEASUREMENTS

A. QD-LED Fabrication

All devices tested in this study are fabricated on top of glass substrates coated with lithographically patterned transparent indium tin oxide (ITO) anodes, on top of which a conducting polymer poly(3, 4-ethylenedioxythiophene):poly(styrenesulfonate) PEDOT:PSS is deposited to facilitate hole injection as well as to minimize ITO surface roughness. We use N,N'-bis(3-methylphenyl)-N,N'-bis(phenyl)benzidine (TPD) as a hole transporting material and tris-(8-hydroxyquinoline) aluminum (Alq_3) as an electron transporting material, as these materials have been extensively studied for OLED applications, and carrier transport and exciton formation in them is well characterized.[11,12] We deposit Mg:Ag cathodes with Ag protective overlayer on top of our structures. Prior to deposition of organics, the ITO coated glass substrates are cleaned in a multistep solvent cleaning process, which is followed by a 5 min exposure to O_2 plasma. PEDOT:PSS films are deposited via spin-coating from an aqueous solution, and then baked at 120 °C for 10 min in a N_2 atmosphere. TPD, Alq_3, and Mg:Ag films are deposited via thermal evaporation at pressures $<5\times10^{-7}$ Torr and rates of 0.15 nm/s. For the emissive

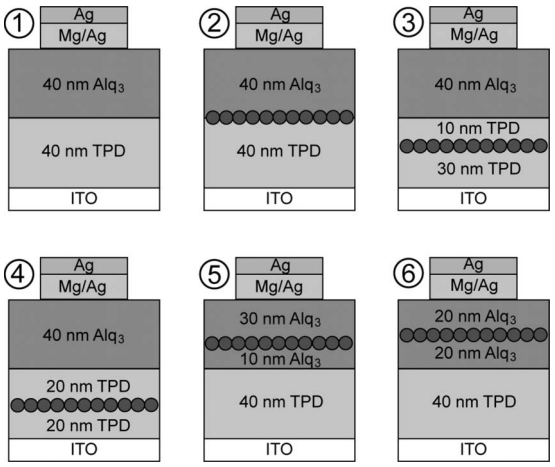

FIG. 1. Schematic of device structures 2, 3, 4, 5, and 6 with the QD monolayer deposited at different positions within the device stack. Device 1 is a control OLED.

monolayers, ZnS overcoated CdSe core-shell QDs with a PL peak at a wavelength $\lambda = 604$ nm and a PL quantum yield of 80% synthesized via established procedures[3] are deposited via microcontact printing. QDs of this type have been previously shown to yield QD-LEDs with relatively high efficiencies of up to 2% in device structures similar to device 2 of Fig. 1.[8]

EQE and current-voltage characteristics measurements are performed in a N_2 glovebox. A HP 2154 measuring unit is used for current measurements and as a voltage source: the same unit in combination with a Newport calibrated photodiode is used to measure light output of QD-LEDs.

Electroluminescence measurements are performed in ambient conditions. Prior to these measurements, all of our devices are packaged in a N_2 atmosphere using glass coverslips sealed to the substrate with UV-curing epoxy. For EL measurements, a Keithley 2600 electrometer is used as a voltage source, and the device EL is coupled into a fiber connected to a Spectra Pro Acton Research spectrometer.

B. Observations

To investigate the contribution of the direct charge injection and exciton energy transfer to QD-LED EL we fabricate the set of devices shown in Fig. 1, in which we vary the position of the emissive QD monolayer within the QD-LED structure. Device 1 is a control OLED,[11,12] and device 2 represents a standard QD-LED structure with a QD monolayer deposited at the interface between the hole and electron transporting layers. In devices 3 and 4, QD monolayers are imbedded into the hole transporting layer 10 nm and 20 nm away from the interface. In devices 5 and 6, QD monolayers are imbedded into the electron transporting layer 10 nm and 20 nm away from the interface.

Figure 5(a) plots the EQE of devices 1 through 6. Device 1 exhibits a peak EQE of 0.8% consistent with previous reports.[11,12] Device 2 shows a peak EQE of 1.5%, which is of the same order of magnitude as in previous reports.[8] Devices 3 and 4 that have a QD monolayer imbedded into the hole transporting layer show higher peak EQEs of 2.3% and 1.7%, respectively, while devices 5 and 6 have peak EQEs of 1.1% and 0.8%. From these results it is evident that imbedding a QD monolayer into the hole transporting layer improves device efficiency by ~50%, while imbedding QDs into the electron-transport layer leads to decreased device efficiency as compared to the standard device 2 structure.

While Fig. 5 presents the data for a single set of QD-LEDs, in order to confirm the reproducibility of the observed trends we fabricated multiple sets of QD-LEDs with the same organic charge transporting materials (TPD and Alq_3) and QDs. We also fabricated other QD-LED sets using N,N'-Bis(3-methylphenyl)- N,N'-bis-(phenyl)-9,9-spiro-bifluorene (spiroTPD) as the hole transporting layer and 2,2′,2″-(1,3,5-Benzinetriyl)-tris(1-phenyl-1-H-benzimidazole) (TPBi) as the electron transporting layer, and different QDs (ZnSe/CdSe/ZnS double-shell QDs emitting at $\lambda = 530$ nm). The absolute efficiency of QD-LEDs from different device sets varies within 25%, as is characteristic for organic LED fabrication. However, within each data set we observe a similar relative efficiency trend, i.e., the efficiency of QD-LEDs increases by 30%–50% upon imbedding QD monolayers into hole transporting layers <10 nm away from the interface of hole and electron transporting layers.

Figure 2 plots the energy-band diagrams for devices 1 through 6. Highest occupied molecular orbital (HOMO) levels of organic materials are obtained from electron photoemission measurements, and the optical-absorption spectroscopy is used to determine relative position of the lowest unoccupied molecular orbital (LUMO) levels.[13] The energy-band structure of QDs is derived numerically by starting with the bulk semiconductor energy-band structure and confining

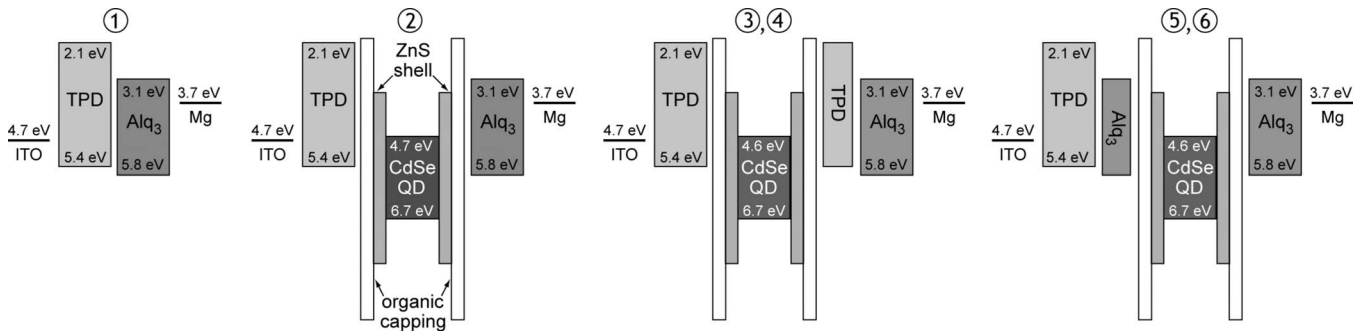

FIG. 2. Suggested energy-band diagrams for devices 1 through 6.

it to the size of the QDs while assuming that carriers in QDs retain the effective mass of bulk semiconductors.[14] It is apparent from Fig. 2 that QDs provide an energy trap for the mobile electrons in the structure, and are not likely to trap holes, due to the high ~1 eV energy barrier for the hole transport from the HOMO levels of TPD and Alq_3 into QDs.

QD charging, due to the accumulation of electrons, can lead to QD luminescence quenching via the nonradiative Auger recombination mechanism.[15] Auger recombination requires the presence of an exciton and an unpaired carrier (electron or hole) at a QD site, which can arise when the concentration of one charge-carrier type is significantly higher than the concentration of the other carrier type at a QD. During Auger recombination, the energy released from the exciton recombination promotes an unpaired carrier to a higher energy level, from which it can thermally relax to its ground state.[16] Auger recombination occurs on the 100 ps time scale,[15] much faster than the radiative recombination lifetime of QDs, which is on the order of 10 ns,[17,18] resulting in the rapid quenching of QD luminescence. Imbedding the QDs into the hole transporting layer can decrease the electron concentration at QD sites and consequently decrease the likelihood of Auger recombination events. This is consistent with the observed increase in QD luminescence efficiency for devices 3 and 4.

III. CONTRIBUTION OF EXCITON ENERGY TRANSFER TO QD-LED ELECTROLUMINESCENCE

Previous studies have demonstrated that thin films of colloidal QDs can efficiently accept excitons from organic thin-film donors, which was manifested as an increase of the QD luminescence intensity in time-resolved photoluminescence experiments.[19] Exciton energy transfer from organic thin films to QDs can also be responsible for QD electroluminescence in QD-LEDs, akin to its contribution in EL of organic light emitting diode (OLED) structures. For example, in the device 1 OLED structure, excitons are formed at the TPD/Alq_3 interface. Due to the higher potential barrier for electron injection from Alq_3 into TPD, as compared to the potential barrier for hole injection from TPD into Alq_3, the majority of excitons are formed on Alq_3 molecules. Furthermore, all excitons formed on TPD molecules can efficiently transfer their energy via the Förster mechanism[20] to Alq_3 molecules because of the spectral overlap of the Alq_3 absorption and TPD emission. This results in an EL spectrum that consists entirely of Alq_3 luminescence (Fig. 3).

Spectral overlap between Alq_3 or TPD emission and QD absorption shown in Fig. 4 suggests the possibility of exciton energy transfer from Alq_3 and TPD to QDs, which would result in the observed narrow QD-LED EL spectra characteristic of colloidal QDs (Fig. 3). Assuming the Förster model[20] we can calculate the Förster radius (R_F), the characteristic distance between a donor and an acceptor at which the rate of the energy transfer becomes equal to that of the donor exciton radiative recombination, from the overlap between the Alq_3 or TPD emission and QD absorption:[20]

$$R_F^6 = \frac{3}{4\pi}\frac{c^4}{n^4}\int \frac{F_D(\omega)\sigma_A(\omega)}{\omega^4}d\omega, \quad (1)$$

where c is the speed of light, $n=1.7$ is the index of refraction of organic thin films, $F_D(\omega)$ is the normalized donor emission spectrum, $\sigma_A(\omega)$ is the acceptor absorption cross section.

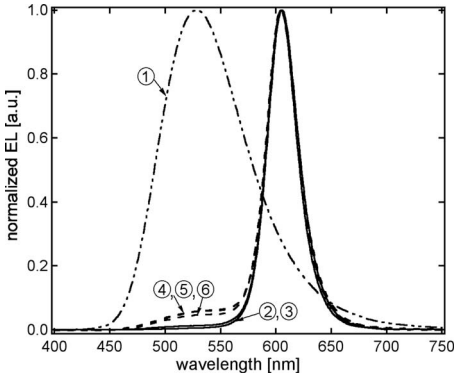

FIG. 3. Normalized EL spectra for devices 1 through 6 are shown at 4 V of applied bias.

Due to the large absorption cross section of each QD, we find R_F to be on the order of 7.5 nm for energy transfer from a single Alq_3 or TPD molecule to a single QD. The exciton energy-transfer rate from a single molecule to a plane of QD acceptors is then obtained by integrating over a QD monolayer:[21]

$$K_{D-AL} = \frac{R_F^6}{\tau}\int_{r=0}^{r=\infty}\frac{2\pi\rho_A r dr}{(r^2+D^2)^3} = \frac{R_F^6}{2a^2D^4\tau} = \frac{1}{\tau}\left(\frac{D_F}{D}\right)^4, \quad (2)$$

where a is the QD radius, τ is the donor PL relaxation time, D is the distance from a donor to a plane of QD acceptors, and D_F is the Förster distance for the energy transfer from a single donor to a plane of acceptors. For energy transfer from the TPD or Alq_3 molecules to a monolayer of QDs ($a=2.5$ nm), we find a Förster distance $D_F \sim 11$ nm. This implies that we should observe substantial energy transfer to QDs of the Alq_3 or TPD excitons formed D_F away from the QD layer. This is in agreement with the QD-LED EL spectra

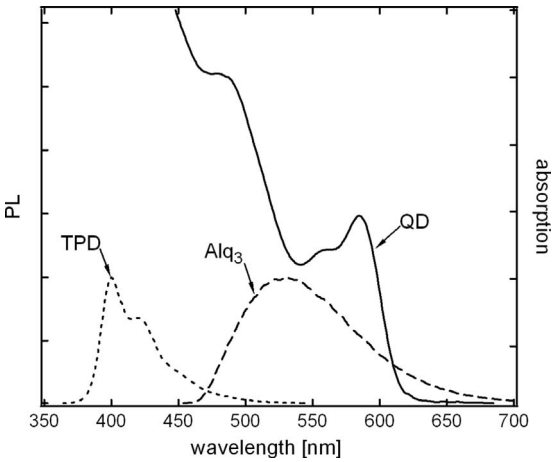

FIG. 4. Photoluminescence spectra of TPD and Alq_3 films are shown together with the absorption spectrum of the colloidal QD solution to demonstrate the large spectral overlap, indicating the likelihood of resonant exciton energy transfer from organic molecules to red colloidal QDs.

displayed in Fig. 3. For devices 2 and 3, that have QDs deposited at the TPD/Alq_3 interface or imbedded 10 nm into the TPD hole transporting layer, we observe no Alq_3 or TPD contribution to the EL spectra, which implies complete energy transfer of the Alq_3 or TPD excitons to the QDs. In devices 4 and 6, 20 nm spacing between the QD monolayer and TPD/Alq_3 interfaces is arguably large compared to the Förster distance of 11 nm for the resonant energy transfer to be observed, nevertheless we only observe small Alq_3 contribution in devices 4 and 6 EL spectra. This can be explained by taking into account the exciton diffusion length on the order of 8 nm in organic thin films.[19,22,23] In devices 4 and 6, excitons formed at TPD/Alq_3 interface have to diffuse prior to energy transfer to the QDs and can recombine on Alq_3 molecules, contributing to Alq_3 spectral signature.

If we assume that exciton energy transfer is the dominant mechanism in QD-LED operation, the observed increase in the QD-LED efficiency upon imbedding the QDs into a hole transporting layer (as in devices 3 and 4) can be accounted for by diminished charge accumulation at the QD sites. Electron transport from Alq_3 to QDs is inhibited by the intervening TPD layer, and hole accumulation at the QDs is unlikely due to the energy-level alignment. This leads to a low probability of exciton transfer to a charged QD, and consequently low occurrence of the Auger quenching process and an increased EQE.

To form excitons on the organic charge transporting layers of QD-LEDs, holes have to be able to travel through the TPD layer to the TPD/Alq_3 interface. The proposed band diagrams of Fig. 2 indicate that hole transport should be impeded in devices 2, 3, and 4 by the presence of the QD monolayer that forms a potential barrier to hole transport. We note, however, that the one-dimensional energy diagrams sketched in Fig. 2, fail to take account of the three-dimensional shape of the QDs. Atomic force microscope images of QD monolayers in QD-LEDs show that 5 nm diameter QDs form hexagonally close-packed monolayers on the TPD surface after microcontact printing,[4] producing nanometer-scale openings between the QD sites. Deposited organic films fill these openings, allowing holes and electrons to pass through the device, bypassing QDs, and reaching the Alq_3/TPD interface where excitons are formed.

In efficient OLEDs, where Auger recombination is negligible and leakage currents are small, higher current densities result in higher exciton formation rates. In less power efficient OLED structures, charge accumulation (at charge trap sites or heterointerface potential steps) results in internal electric fields driving charge in the opposite direction to the applied bias voltage. This leads to lower space-charge limited currents[24,25] at a given externally applied voltage and, consequently, to lower exciton formation rates. Similarly, charge transport in QD-LEDs is also governed by the properties of the organic charge transporting layers, so that space-charge limited conduction[24,25] is the dominating conduction mechanism. Since QDs trap electrons efficiently, we expect electron accumulation at QD sites, which contributes to space-charge buildup and results in lower currents through the device at a given external bias, lower exciton formation rates, and higher Auger loss rates at the QD sites. These effects would be manifested as reduced QD-LED EQE. Performance of devices 2, 5, and 6 is consistent with this analysis, as they demonstrate lower current densities at a given bias voltage [Fig. 5(b)] and lower EQEs [Fig. 5(a)] as compared to devices 3 and 4.

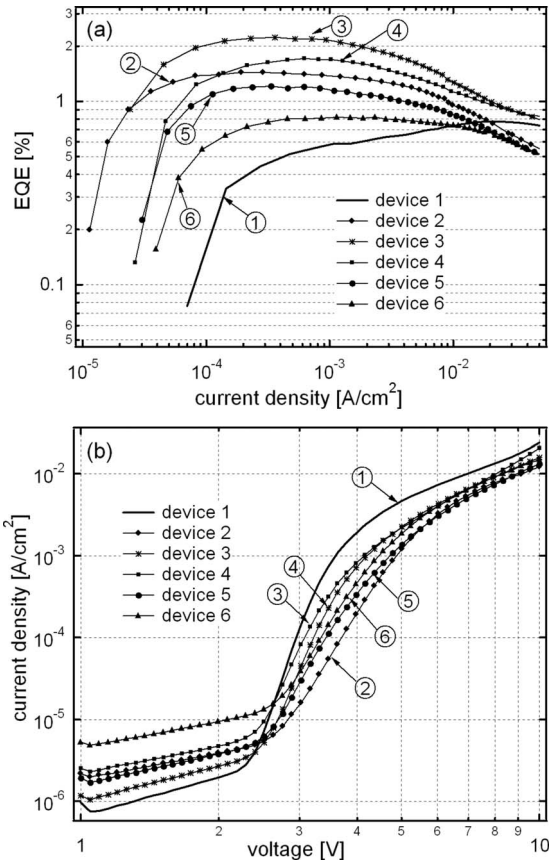

FIG. 5. (a) EQE measured for devices 1 through 6 as a function of current through each device. (b) Current-voltage characteristics for devices 1 through 6.

It is assumed in the analysis above that the leakage currents through the devices are small, which is supported by the OLED EQE value that is consistent with previous reports. High leakage currents resulting from short circuit pathways through the device typically caused by morphological defects impede the device efficiency, as they do not contribute to the device EL. In order to compare the exciton generation in different LED structures it is essential to fabricate the devices in a parallel process, conserving the design parameters so that internal morphology is consistent from one device to another.

IV. CHARGE TRANSPORT AND EXCITON FORMATION

While the experiment described above provides the evidence of the contribution of exciton energy transfer to the QD-LED operation, the observed trends also appear consistent with the direct charge injection model of QD-LED operation. The increase in the QD-LED EQE upon imbedding the QDs into a hole transporting layer as in device 3 and 4 may imply better electron and hole balance. In these structures electrons travel through a thin hole-transport layer be-

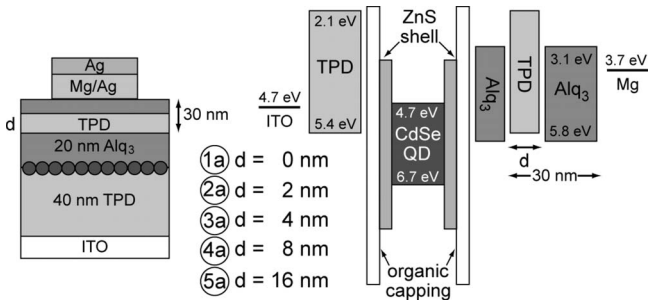

FIG. 6. Schematic device structure for devices 1a through 5a. Thickness of the TPD electron blocking barrier, d, is varied for the devices, while the total thickness of the electron transporting layer is kept equal to 50 nm, and the TPD blocking layer is separated by 20 nm of Alq_3 from the QD monolayer. $d=0$ nm for device 1a, $d=2$ nm for device 2a, $d=4$ nm for device 3a, $d=8$ nm for device 4a, $d=16$ nm for device 5a.

fore reaching QDs, which slows down electron arrival to the QD sites, lowering the number of electron-exciton pairs at QDs, reducing the occurrence of Auger recombination events, and therefore increasing the overall QD luminescence efficiency. Conversely, imbedding QDs into an electron transporting layer, as in device 5 and 6, leads to an increase in the electron concentration at QD sites. This results in higher probability of formation of the electron-exciton pairs and decreased QD-LED efficiency. In order to test the "charge balance" hypothesis and to investigate electron transport in QD-LEDs, we fabricate QD-LED structures shown in Fig. 6. In these structures, we insert a TPD electron blocking layer (EBL) inside the Alq_3 electron transporting layer and vary the thickness of this TPD layer from 0 to 16 nm. The presence of the barrier to the electron transport may result in a reduced electron concentration at QD traps, leading to more balanced electron and hole concentrations at the QD sites and consequently reduced formation of undesirable electron-exciton pairs.

All the devices of Fig. 6 are fabricated on glass substrates and have an ITO anode with a PEDOT:PSS hole injecting layer, a 40 nm TPD layer for hole transport, and an emissive colloidal QD monolayer deposited via microcontact printing.[4] The 50 nm electron transporting layer consists of Alq_3 for device 1a. For the remaining devices, the electron transporting layer is built of 20 nm thick Alq_3 film on top of QD monolayer followed by the TPD EBL of varying thickness and an Alq_3 layer with its thickness chosen to result in an electron transporting layer with a total thickness of 50 nm. Mg:Ag cathodes are deposited on top of the structures.

Figure 7(a) shows the EQEs for devices 1a through 5a. Devices 1a, 2a, and 3a have EQEs of 1.8%, 1.7%, and 1.6%, respectively. The EQE of device 4a is ~1% and device 5a is the least efficient with an EQE of ~0.14%. The current-voltage characteristics [Fig. 7(b)] for devices 1a through 5a show that device 1a is the least resistive and device 5a is the most resistive. The resistance of the devices increases with increasing thickness of the electron blocking TPD layer, which is in agreement with the device structures and band diagrams of Fig. 6 that illustrate increasingly impeded electron transport with the increasing thickness of the inserted

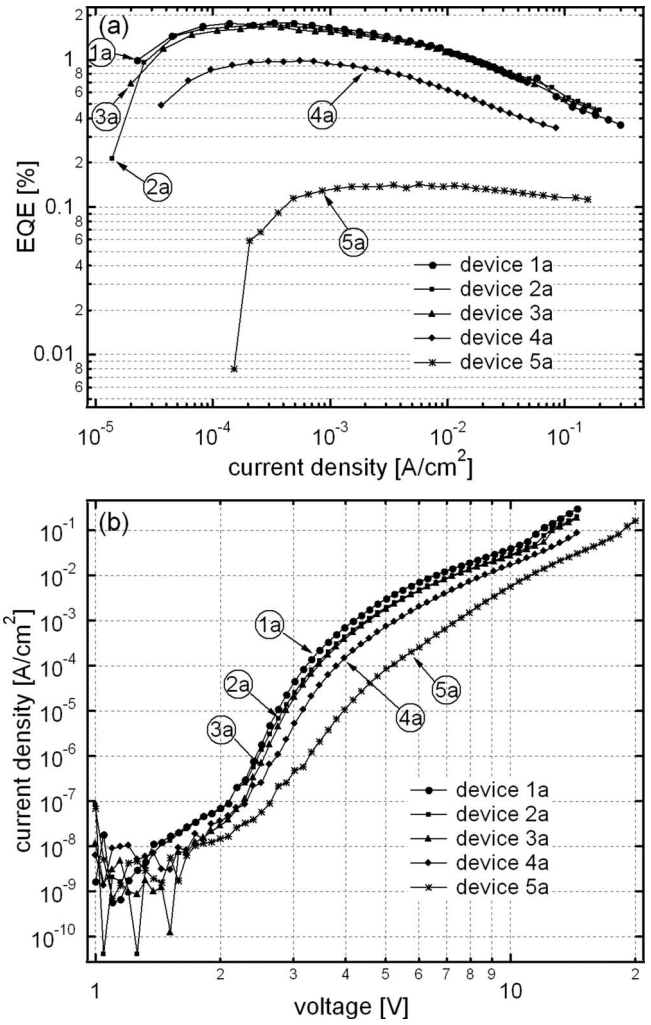

FIG. 7. (a) EQE of devices 1a (circles), 2a (squares), 3a (triangles), 4a (diamonds), and 5a (stars) as a functions of the current density through each device. (b) Current-voltage characteristics for devices 1a (circles), 2a (squares), 3a (triangles), 4a (diamonds), and 5a (stars).

TPD layer. However, the decrease of the EQE with increasing thickness of the inserted TPD layer is unexpected: the inserted TPD layer should improve the balance of electron and hole densities at QD sites, reducing the Auger process and increasing EQE.

We also performed repeated EQE measurements on each of the devices of Fig. 6, using four measurement cycles with 30 s interval between the cycles [Fig. 8(a) plots]. For devices 1a, 2a, and 3a, we find a nearly 50% decrease in EQE from the first to the second measurement, with an additional ~20% decrease in EQE on the third measurement cycle, and ~10% decrease on the fourth cycle. A smaller decrease in EQE is observed for the sequence of measurements on device 4a (~40% decrease on the second measurement, ~10% on the third, and ~5% on the fourth cycle); while for device 5a there is no noticeable change of EQE with consecutive measurement cycles. We also notice that EQE of the originally most efficient device 1a decreases the most in the second, third, and fourth cycles, which makes it less efficient in those cycles than device 2a and 3a.

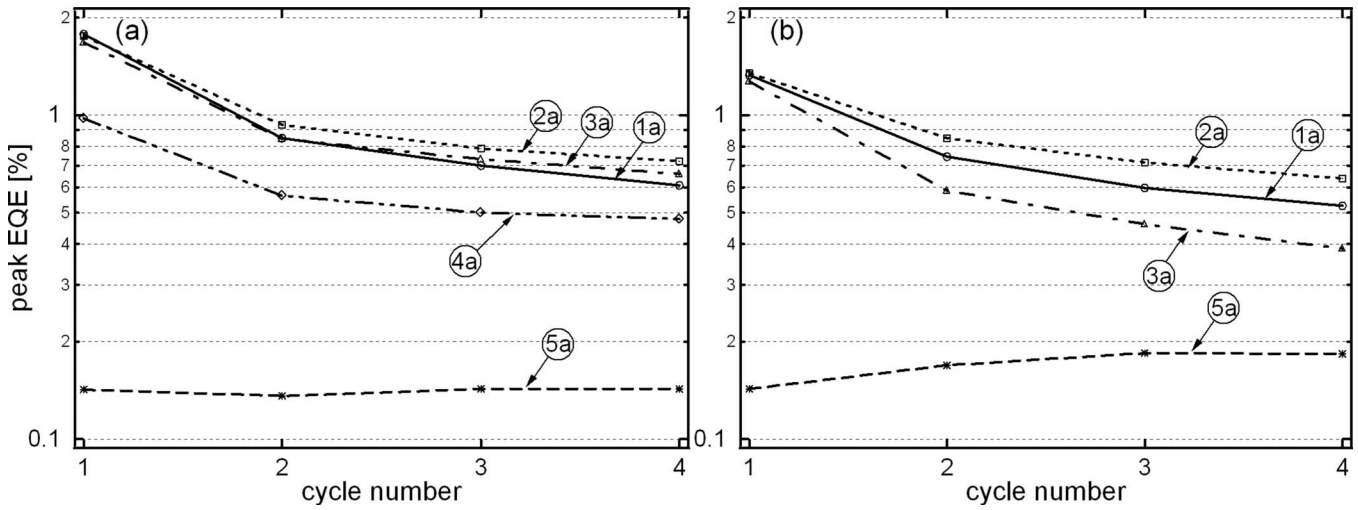

FIG. 8. (a) Peak EQE for devices 1a through 5a, taken in four consecutive measurements cycles separated by ~30 s. In every measurement, the cycle bias voltage is scanned from 1 to 15 V (devices 1a through 4a) or from 1 to 20 V (device 5a). (b) Peak EQE for devices 1a, 2a, 3a, and 5a measured in an experiment identical to the one in (a) performed on a next day.

We repeated the test cycling of our devices on the following day and found EQEs nearly the same as for the fresh devices [Fig. 8(b)], prior to cycling. The observed decrease in EQE of the cycled devices, and subsequent recovery after one day wait period, can therefore be attributed to the charging of the QD monolayer with excess electrons during operation, and a slow release of charge that was trapped on the QDs as the devices rested for one day.

Charging of the QDs in the QD-LED structure contributes to the decrease in EQE, and from the above cycling experiment it is apparent that structures 2a through 5a reduce the QD charging as compared to device 1a, with the most pronounced decrease in charging observed for devices 4a and 5a. However, while we can controllably eliminate electron accumulation at the QD sites in these structures, we do not observe an increase in QD-LED efficiency upon inserting thicker TPD EBL into the Alq_3 layer. Instead, QD-LED peak efficiency is the lowest for devices 4a and 5a.

To explain the observed data, we note that the EQEs of these devices are not solely governed by the QD charging but also by exciton generation. Charge accumulation in Alq_3 at a TPD EBL interface located closer to the cathode results in a decreased current through the device and consequently decreased exciton formation. The thin TPD EBL of devices 2a and 3a does not lead to a significant charge accumulation at the Alq_3/TPD interface and consequently does not have a major impact on the peak EQE. The thick TPD EBL of devices 4a and particularly 5a significantly impedes electron transport through these devices (which is in agreement with IV characteristics of Fig. 7(b) that show higher resistance for these devices) reducing exciton formation and consequently lowering the EQE.

Another important factor contributing to QD-LED EQE is the distribution of internal electric fields within a structure. It has been previously demonstrated that in the structures that incorporate single QDs into hole transporting organic thin films, the field induced exciton dissociation is the primary mechanism of QD luminescence quenching.[26] In those structures QD charging is not expected to significantly contribute to QD luminescence quenching since QDs are well separated from each other providing low resistance pathways for the carrier transport. Additionally the current in those devices is dominated by holes that are not trapped efficiently by QDs. In the present study, close-packed QD monolayers provide an electron trap (see Figs. 2 and 6), and the proximity of electron transporting layer results in high probability of an electron capture by QDs. While incorporating TPD EBL may cause a change in the distribution of internal electric fields in QD-LED structures, it is unlikely that the field across the QD monolayer will change by the several orders of magnitude needed to significantly impact the exciton dissociation rate. Consequently the QD charging with electrons is expected to have a more dramatic effect on the QD luminescence efficiency in our devices.

To investigate the exciton formation mechanism in devices 2a through 5a, we perform EL measurements at different applied bias conditions (Fig. 9). The EL for devices 2a through 4a was measured at bias voltages between 3 and 15 V, and for the device 5a at bias voltages between 6 and 20 V, since this device has a significantly higher resistance and turn-on voltage. Figure 9 shows normalized EL spectra for each of the devices divided into two groups. The first set of EL spectra [Figs. 9(a), 9(c), 9(e), and 9(g)] corresponds to the voltages at which the EL intensity increases with increasing applied bias voltage. The second set [Figs. 9(b), 9(d), 9(f), and 9(h)] corresponds to the voltages at which the EL intensity decreases with increasing applied bias. All the devices reach maximum brightness at similar driving current densities $J \sim (3 \pm 1)$ mA/cm^2. This current density corresponds to 9 V for device 2a, 11 V for device 3a, 12 V for device 4a, and 15 V for device 5a. The decrease of the EL intensity with higher applied currents (voltages) is atypical of OLEDs, and in these QD-LED structures can be caused by the charge accumulation at QD sites and TPD (EBL)/Alq_3 interface.

We also notice that the contribution of the Alq_3 emission to the device EL spectra increases consistently with increas-

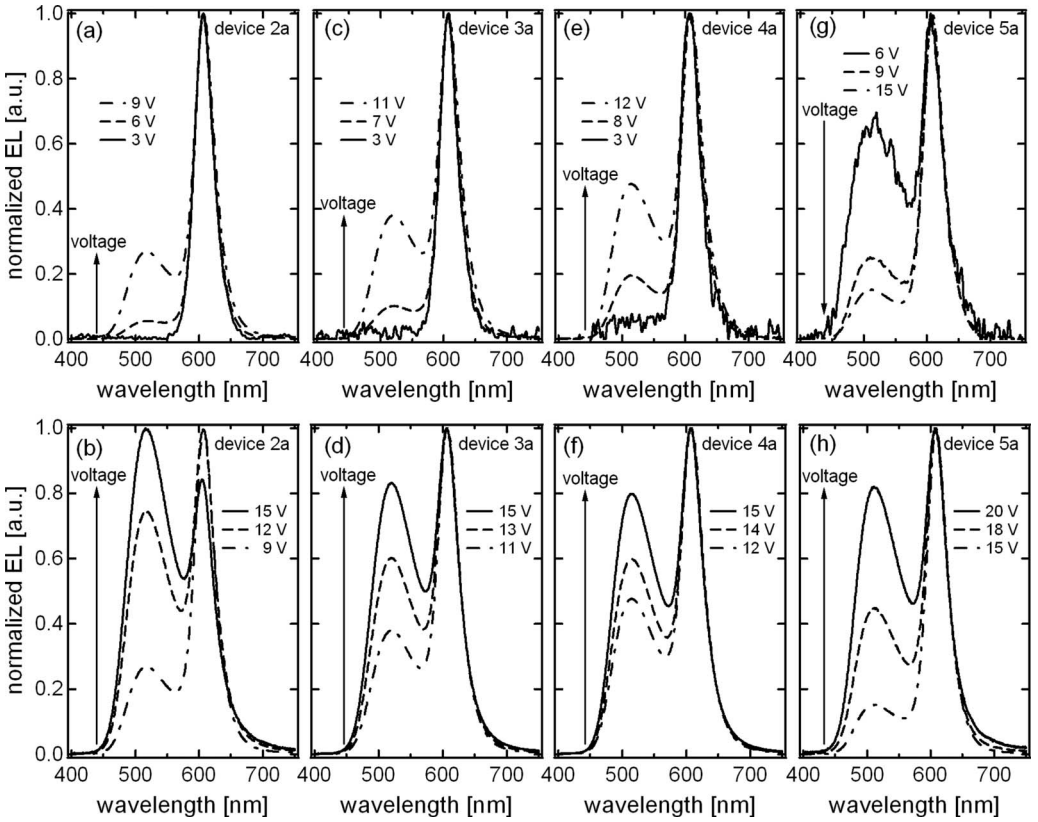

FIG. 9. (a), (c), (e), and (g) Normalized EL spectra for devices 2a, 3a, 4a, and 5a taken at different bias voltages. The EL intensity increases with increasing applied bias. (b), (d), (f), and (h). Normalized EL spectra for devices 2a, 3a, 4a, and 5a taken are at different bias voltages. In these plots, the EL intensity decreases with increasing applied bias. The arrow shows the direction of the increasing bias voltage.

ing applied bias for devices 2a, 3a, and 4a. For device 5a EL spectra, we first observe a decrease in Alq_3 component at bias voltages between 6 and 13 V, followed by an increase at bias voltages above 13 V akin to that of the devices 2a through 4a. The evolution of EL spectra appears consistent with the energy-transfer model and can be explained by the position of exciton formation region within the devices. In devices 2a, 3a, and 4a, where the TPD EBL is sufficiently thin for electrons to transport through, the majority of excitons form in the Alq_3 layer next to a QD monolayer, from where they resonantly transfer to QDs. At higher currents through the device, the concentration of electrons at QD sites significantly increases, leading to the Auger-facilitated quenching of the QD emission. In addition, the exciton generation region becomes wider, occupying larger volume of Alq_3. Consequently some excitons form further than a D_F away from the QD monolayer, which increases the probability of their radiative recombination on Alq_3 molecules.[27] In the device 5a, where the TPD EBL is thick, at lower bias voltages, the majority of electrons slowed down by the barrier do not reach the Alq_3/QD interface. Consequently, the exciton formation region is shifted toward the Alq_3/TPD (EBL) interface, which is more than $2D_F$ away from the QD monolayer. This leads to significant radiative recombination of the excitons on the Alq_3 molecules. At higher bias voltages, electrons have a higher probability of reaching the Alq_3/QD interface, contributing to exciton generation near QD sites and hence more efficient energy transfer and higher QD emission intensity. At very high bias voltages >13 V we observe the same trend as for devices 2a, 3a and 4a, where the exciton formation region at higher bias voltages occupies the bulk of Alq_3 layer adjacent to QDs.

The spectral purity of QD-LED emission is very sensitive to the device structure and can differ with respect to different fabrication methods. Factors such as the closeness of QD-to-QD packing of the QD monolayer or the number of QD monolayers in the QD-LED structure have a significant impact on QD-LED EL spectra. The morphology of a monolayer depends on a QD size distribution and an average QD size, i.e., smaller QDs tend to provide denser films. In archetypical QD-LED structures, akin to device 1a in Fig. 6, organic components of EL spectra tend to increase with increasing bias voltage,[27] however, this effect may not be apparent at low voltages ($<10-15$ V) in devices with high QD packing density or multiple QD layers. In order to investigate exciton generation regions in QD-LEDs, in this study we only compare devices fabricated in parallel that have identical design parameters such as QD film morphology.

V. CONCLUSION

Our experiments suggest that charging of the QDs with electrons significantly contributes to decrease of QD-LED efficiency. One method to improve the performance of these devices is to imbed the luminescent QD monolayer into a hole transporting layer ≤ 10 nm away from the exciton-

generating interface. We also suggest that resonant energy transfer contributes significantly to device performance, and exciton formation within the Förster distance away from the QD monolayer can increase device efficiency. Having precise control over the position of the exciton formation region enabled us to monitor energy transfer processes within the device structure, which is crucial for the applications where the contribution to the EL spectrum by each emitter type is important. While exciton formation through direct charge injection could potentially lead to more efficient devices (as this process eliminates exciton losses associated with incomplete energy transfer), it calls for a precise electron and hole concentration balance and a similar barrier for electron/hole injection into QDs. In case of a charge imbalance, or if one carrier is trapped by QDs more efficiently than the other, the EQE of the device would be reduced by QD charging and consequent Auger recombination. Designing devices that rely on precise charge balance and exciton formation on QDs can be difficult and requires a hole transporting material with lower HOMO level than the QD valence band and a band gap larger than that of QDs. Designing devices that mostly rely on the exciton generation within the organic layers and their resonant transfer to QDs does not require design and synthesis of new organic materials and provides an opportunity to use efficient donors (such as phosphorescent materials) for the exciton generation and a subsequent transfer to QDs.

ACKNOWLEDGMENTS

The authors would like to thank S. A. Coe-Sullivan for insightful discussions. The work was supported in part by the NSF-MRSEC Program (DMR-0213282), making use of its Shared Experimental Facilities, the U.S. government, and the U.S. Army through the Institute for Soldier Nanotechnolgies (DAAD-19-02-0002).

*Present address: TJet Technologies, Inc., Menlo Park, CA, USA.

[1] S. Coe, W.-K. Woo, M. G. Bawendi, and V. Bulović, Nature (London) **420**, 800 (2002).
[2] C. B. Murray, D. J. Norris, and M. G. Bawendi, J. Am. Chem. Soc. **115**, 8706 (1993).
[3] B. O. Dabbousi, M. G. Bawendi, O. Onitsuka, and M. F. Rubner, Appl. Phys. Lett. **66**, 1316 (1995).
[4] L. Kim, M.S. thesis, Massachusetts Institute of Technology, 2006.
[5] S. A. Coe-Sullivan, Ph.D. thesis, Massachusetts Institute of Technology, 2005.
[6] P. O. Anikeeva, J. E. Halpert, M. G. Bawendi, and V. Bulović, Nano Lett. **7**, 2196 (2007).
[7] J. S. Steckel, S. Coe-Sullivan, V. Bulović, and M. G. Bawendi, Adv. Mater. (Weinheim, Ger.) **15**, 1862 (2003).
[8] S. Coe-Sullivan, J. S. Steckel, W.-K. Woo, M. G. Bawendi, and V. Bulović, Adv. Funct. Mater. **15**, 1117 (2005).
[9] J. Zhao, J. A. Bardecker, A. M. Munro, M. S. Liu, Y. Niu, I.-K. Ding, J. Luo, B. Chen, A. K.-Y. Jen, and D. S. Ginger, Nano Lett. **6**, 463 (2006).
[10] Y. Li, A. Rizzo, R. Cingolani, and G. Gigli, Adv. Mater. (Weinheim, Ger.) **18**, 2545 (2006).
[11] C. W. Tang and S. A. VanSlyke, Appl. Phys. Lett. **51**, 913 (1987).
[12] C. W. Tang, S. A. VanSlyke, and C. H. Chen, J. Appl. Phys. **65**, 3610 (1989).
[13] H. Ishii, K. Sugiyama, and K. Seki, Proc. SPIE **3148**, 228 (1997).
[14] Al. L. Efros and M. Rosen, Annu. Rev. Mater. Sci. **30**, 475 (2000).
[15] V. I. Klimov, A. A. Mikhailovsky, D. W. McBranch, C. A. Leatherdale, and M. G. Bawendi, Science **287**, 1011 (2000).
[16] P. T. Landsberg, *Recombination in Semiconductors* (Cambridge University Press, Cambridge, 2003).
[17] M. Nirmal, D. J. Norris, M. Kuno, M. G. Bawendi, Al. L. Efros, and M. Rosen, Phys. Rev. Lett. **75**, 3728 (1995).
[18] C. R. Kagan, C. B. Murray, M. Nirmal, and M. G. Bawendi, Phys. Rev. Lett. **76**, 1517 (1996).
[19] P. O. Anikeeva, C. F. Madigan, S. A. Coe-Sullivan, J. S. Steckel, M. G. Bawendi, and V. Bulović, Chem. Phys. Lett. **424**, 120 (2006).
[20] Th. Förster, Ann. Phys. **437**, 55 (1948).
[21] H. Kuhn, J. Chem. Phys. **53**, 101 (1970).
[22] E. B. Namdas, A. Ruseckas, I. D. W. Samuel, S.-C. Lo, and P. L. Burn, Appl. Phys. Lett. **86**, 091104 (2005).
[23] N. Matsusue, S. Ikame, Y. Suzuki, and H. Naito, Appl. Phys. Lett. **97**, 123512 (2005).
[24] A. Rose, Phys. Rev. **97**, 1538 (1955).
[25] M. A. Lampert, Phys. Rev. **103**, 1648 (1956).\
[26] H. Huang, A. Dorn, G. Nair, V. Bulovic, and M. G. Bawendi, Nano Lett. **7**, 3781 (2007).
[27] S. Coe-Sullivan, W.-K. Woo, J. S. Steckel, M. G. Bawendi, and V. Bulovic, Org. Electron. **4**, 123 (2003).